

RSC Advances



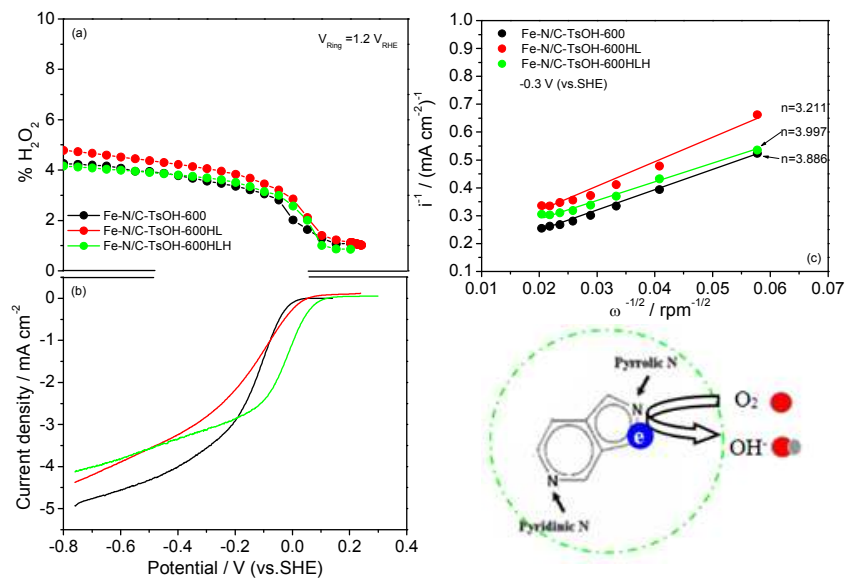
This is an *Accepted Manuscript*, which has been through the Royal Society of Chemistry peer review process and has been accepted for publication.

Accepted Manuscripts are published online shortly after acceptance, before technical editing, formatting and proof reading. Using this free service, authors can make their results available to the community, in citable form, before we publish the edited article. This *Accepted Manuscript* will be replaced by the edited, formatted and paginated article as soon as this is available.

You can find more information about *Accepted Manuscripts* in the [Information for Authors](#).

Please note that technical editing may introduce minor changes to the text and/or graphics, which may alter content. The journal's standard [Terms & Conditions](#) and the [Ethical guidelines](#) still apply. In no event shall the Royal Society of Chemistry be held responsible for any errors or omissions in this *Accepted Manuscript* or any consequences arising from the use of any information it contains.

Graphical Abstract



Nitrogen/sulfur co-doped non-novel metal material as an efficient electrocatalyst for oxygen reduction reaction in alkaline media

Nitrogen/sulfur co-doped non-noble metal material as an efficient electrocatalyst for the oxygen reduction reaction in alkaline media

Cite this: DOI: 10.1039/x0xx00000x

Li Xu,^{*ab} Guoshun Pan^{*ab} and Xiaolu Liang^{ab}

Received 17th February 2014,
Accepted 00th February 2014

DOI: 10.1039/x0xx00000x

www.rsc.org/

This work demonstrates the feasibility of nitrogen/sulfur co-doped non-noble metal materials (Fe-N/C-TsOH) as platinum-free catalysts for the oxygen reduction reaction (ORR) in alkaline media. Electrochemical techniques such as cyclic voltammetry (CV), rotating disk electrodes (RDE) and rotating ring-disk electrode (RRDE) are employed with the Koutecky-Levich theory to investigate the ORR kinetic constants and the reaction mechanism. It is found that the catalysts doped with TsOH (p-toluenesulfonic acid) show significantly improved ORR activity relative to a TsOH-free catalyst. The overall electron transfer numbers for the catalyzed ORR are determined to be 3.899 and 3.098, respectively, for the catalysts with and without TsOH-doping. Catalysts heat treated at 600°C exhibit relatively higher activity. In addition, the catalyst doped with TsOH (Fe-N/C-TsOH-600) not only exhibits exceptional stability in 0.1 mol L⁻¹ KOH solution but also has higher methanol tolerance compared to commercial Pt/C catalyst in 0.1 mol L⁻¹ KOH. To some extent, increasing the Fe-N/C-TsOH-600 loading on the electrode favors a faster reduction of H₂O₂ to intermediate to H₂O. X-ray photoelectron spectroscopy analysis indicates that pyrrolic N groups are the most active sites, and that sulfur species are structurally bound to carbon in the forms of C-S_(n)-C and oxidized -SO_(n)- bonds, an additional beneficial factor for the ORR.

1. Introduction

Polymer electrolyte membrane (PEM) fuel cells are considered a promising technology to replace internal combustion engines for automotive propulsion, due to their high energy yield and low environmental impact. Notable among these are direct methanol alkaline fuel cells (DMAFCs), which have attracted considerable interest as alternative power sources for automobiles and portable consumer electronics.¹ Since alcohols have a similar distribution infrastructure to petroleum, they can be easily handled, stored, and transported, and they promise major improvements over gasoline combustion, including better overall fuel efficiency and lower emissions.² Nevertheless, the sluggish kinetics of the cathodic ORR is a major factor hampering large-scale implementation of DMAFCs, so most research in this area currently focuses on developing efficient catalysts for the ORR.³

The ORR process can occur along a 4-electron pathway to directly produce H₂O or a less efficient 2-electron pathway involving the formation of H₂O₂ as an intermediate.^{4,5} Although platinum-based nanomaterials are the most efficient ORR catalysts, they still face multiple problems, such as unstable catalytic activity, poor stability, limited supply, and high cost.⁵⁻⁷ As well, due to anode methanol penetration, oxygen reduction and methanol oxidation occur simultaneously on the Pt surface, forming “cathodic mixed potential” and decreasing the cell performance as well as poisoning the cathode catalyst's Pt.⁸⁻¹⁰ Thus, developing cost-effective catalysts with high ORR catalytic activity, long-term stability, and methanol tolerance is crucial for advancing DMAFCs.

Owing to the inherently faster electrode kinetics and less

corrosive conditions in alkaline media, a large number of catalysts have been investigated for the ORR in DMAFCs. Catalysts synthesized by pyrolyzing precursors comprising nitrogen, carbon, and transition metals have drawn significant attention because of their reasonable activity levels, remarkable selectivity in the catalysis of the ORR, and high tolerance to methanol, even though the mechanisms of the catalyst reaction during the heat-treatment process and the resulting improvement in activity are complicated and not fully understood.^{2, 11-13} Chu and Jiang^{14,15} prepared a series of single and binary heat-treated metalloporphyrins (TPP as a ligand), and tested the ORR in O₂-saturated 0.5 mol L⁻¹ H₂SO₄ with 1 mol L⁻¹ methanol. The best catalyst for oxygen reduction, which was also inert to methanol oxidation, was heat-treated Co-/Fe-TPP. Chu and Jiang proposed that the macrocycles were only partially decomposed

by the heat treatment (600°C in Ar), the carbonized organic groups could form a nanostructure and the catalytic sites were MN₄ core. Holze *et al.* investigated carbon-supported Fe-TMPP (TMPP stands for tetramethoxyphenylporphyrin) heated treated at 800°C as an active catalyst for the ORR in fuel cells using methanol as the fuel and an alkaline carbonate electrolyte.¹⁶ The pyrolyzed Fe-TMPP catalyst was as active as Pt/C and less sensitive toward the establishment of a mixed potential. Indeed, upon the addition of 1 mol L⁻¹ methanol, the polarization curve of the chelate-load electrode remained unchanged, whereas the Pt/C electrode showed much poorer performance.

Very recently, carbons doped or co-doped with other heteroatoms, such as B,¹⁷ P,^{18,19} and S,^{20,21} have been developed and have shown good catalytic activity for the ORR by taking advantage

of the different heteroatoms in the conjugated carbon backbone that can create new non-electroneutral sites. For instance, S and N co-doped carbons have shown better tolerance to methanol than commercial Pt/C electrode.²² Nevertheless, some parameters, such as onset potential, half-wave potential, and current density, still need to be improved.

In this work, TsOH and polypyrrole (PPy) were used as dual dopants to synthesize a novel non-precious metal catalyst, Fe-N/C-TsOH. TsOH, an organic compound, is known as a tosyl group and was used not only as the S precursor but also as an "organic-soluble" acid catalyst to promote the oxidation of pyrrole. ORR activity and methanol tolerance were assessed using CV, RDE and RRDE techniques. Powder X-ray diffraction (XRD) as well as X-ray photoelectron spectroscopy (XPS) were employed to confirm the material properties in terms of morphology and chemical speciation. We demonstrated that the catalyst doped with TsOH showed much better electrocatalytic activity for ORR performance than a catalyst without TsOH doping. We then focused on evaluating Fe-N/C-TsOH catalyst heat treated at 600°C. In particular, the effect of KOH concentration on its ORR catalytic properties was examined using the RRDE technique in 0.1–5.0 mol L⁻¹ KOH electrolyte. The effect of heat treatment on the catalyst's methanol tolerance was studied, and we compared this tolerance with that of commercially available Pt/C to evaluate the treated catalyst's applicability in DMAFCs.

2. Experimental

2.1. Preparation and physical characterization of the catalysts

To prepare the nitrogen and sulfur dual-doped non-precious metal electrocatalyst (Fe-N/C-TsOH), we mixed 50 mg pyrrole (chemically pure) and 10 mL methanol solvent (analytically pure; both purchased from Guoyao, Shanghai), then combined this mixture with 120 mg carbon black (Vulcan XC 72R with a BET of 235 m² g⁻¹, purchased from Cabot), followed by 10 min of ultrasonication. 0.25 mL 30% H₂O₂ and 50 mg TsOH (analytically pure, purchased from Guoyao) were added to this ultrasonicated suspension while being ground in a mortar for some time to obtain a slurry. 10 mL methanol with 149 mg FeSO₄·7H₂O (analytically pure) was then added to the mortar, followed by constant milling for another 45 min, then drying in a vacuum at 60°C for 1 h to obtain a powder. This powder was further processed by thermal treatment under N₂ atmosphere at temperatures of 200, 400, 600, and 700°C, respectively, for 2 hours to optimize the pyrolysis temperature with respect to ORR electrocatalytic activity. To elucidate the effect of TsOH alone, a baseline sample of carbon loaded with TsOH-free Fe-N was also prepared under the same conditions described above and is denoted as Fe-N/C. Furthermore, the Fe-N/C-TsOH-600 catalyst was leached in 0.5 mol L⁻¹ H₂SO₄ at 80 to 90°C for some hours to remove excess metals on the surface of the catalyst (denoted as Fe-N/C-TsOH-600L). Then the resulting samples were filtered, washed, and subjected to a second heat treatment at 600°C under N₂ for 2 h (denoted as Fe-N/C-TsOH-600LH). In the relevant figure's legend, "RT" means untreated or unpyrolyzed catalyst and "600" indicates the sample pyrolyzed at 600°C.

Structural and crystal-phase analyses of the catalysts were performed using XRD with Cu K α radiation ($\lambda = 0.15406$ nm), operating at 40 kV and 40 mA. Surface analysis of the catalysts was conducted by XPS on a PHI Quantera Scanning X-ray MicroprobeTM 5300 system (ULVAC-PHI, INC) with an Al K X-ray anode source ($h\nu = 1486.6$ eV) at 300 W and 15.0 kV.

2.2. Electrochemical measurements

Electrochemical measurements were performed in a conventional three-electrode cell using the RRDE technique in KOH solution, ranging in concentration from 0.1 to 5.0 mol L⁻¹, at room temperature. A rotating glassy carbon disk electrode (glassy carbon electrode with a geometric surface area of 0.19625 cm², purchased from Gamry Instruments) was coated with catalyst to form the catalyst layer and functioned as the working electrode. According to the electrode preparation method described by Qiao *et al.*,² aliquots of 5, 10, 20, 30, and 40 μ L of homogeneous catalyst ink, consisting of 2.0 mg catalyst mL⁻¹, were pipetted onto the glassy carbon (GC) disk electrode. The catalyst loadings were 50.9, 101, 203.6, 305.4, and 407.2 μ g cm⁻². A saturated calomel electrode (SCE) and Pt wire were used as the reference and counter electrodes, respectively. All measured potentials were converted to the standard hydrogen electrode (SHE).

During the measurement, CVs were first carried out on the freshly prepared working electrode by repeatedly cycling the potential between 0.80 and 0.30 V for more than 30 cycles at a scan rate of 50 mV s⁻¹ in the presence of N₂ bubbling. In this case, the electrode surface was determined to be clean when a stable, reproducible voltammogram was recorded. The ORR activity of the catalyst was tested in O₂-saturated KOH solutions. For more quantitative measurements of the ORR activity, linear sweep voltammetry (LSV) was conducted on the catalyst-coated RDE in the potential range between 0.76 and 0.15 V at a scan rate of 5 mV s⁻¹ in O₂-saturated KOH solution at various rotation rates, from 300 to 2100 r min⁻¹.

3. Results and discussion

3.1. Electrochemical activity of Fe-N/C-TsOH catalysts towards the ORR

LSV measurements of the catalysts prepared without and with TsOH in O₂-saturated 0.1 mol L⁻¹ KOH solutions were taken at 5 mV s⁻¹, and the results are presented in Fig. 1. Both Fe-N/C-TsOH-600 and Fe-N/C-600 are catalytically active for the ORR. However, Fe-N/C-TsOH-600 gives much higher ORR activity than Fe-N/C-600 if both their onset potentials (E_{onset}) and their half-wave potentials ($E_{1/2}$) are compared. In addition, the maximum current density for Fe-N/C-TsOH-600 is 1.7 times higher than that of Fe-N/C-600. In other words, the addition of TsOH considerably enhances the former catalyst's activity relative to the latter's. According to the literature, the dopant breaks the electroneutrality of the carbon material, since the difference in electroneutrality between carbon and dopant creates favorable positively charged sites for side-on O₂ surface adsorption.¹⁷ As well, pyrolysis of the catalyst in the presence of sulfur leads to mainly amorphous carbon, resulting in increased catalyst porosity and, in turn, enhanced catalyst performance.^{23,24} Furthermore, sulfur (or a sulfo group), whose electronegativity is close to that of carbon, has been employed as a dopant in the preparation of M-N_x catalysts, and the sulfur group doped to M-N_x-C might be helpful for entrapping M ions in an environment rich in pyrrole-type or pyridine-type nitrogen.²⁰

The difference between the diffusion-limiting currents of Fe-N/C-TsOH-600 and Fe-N/C-600 may suggest that the ORR mechanisms they catalyze are different, particularly in terms of the overall electron transfer number. The inset graph in Fig. 1 shows CVs of the two catalysts, which reinforce the LSV results. A more positive peak potential value and a higher peak current density were obtained than with Fe-N/C-600, indicating better ORR activity after TsOH-doping. We therefore believe

that the TsOH or the sulfur plays a key role in improving the electrocatalytic performance of these carbon materials for the ORR.

For a more quantitative evaluation of the ORR catalytic activity of the dual-doped catalysts developed in this work, further RDE voltammetry measurements were carried out at different electrode rotation rates, from 300 to 2100 r min⁻¹, as shown in Fig. 2(a) and (b). The overall electron transfer number (*n*) during the ORR process can be evaluated from the Koutecky-Levich equation:²

$$i_d^{-1} = i_k^{-1} + (0.201nFC_{O_2}D_{O_2}^{2/3}v^{-1/6}\omega^{1/2})^{-1} \quad (1)$$

where i_d is the disk ORR current density, i_k is the kinetic current density, n is the overall number of electrons transferred per molecule of O₂ reduced, F is Faraday's constant ($F = 96485 \text{ C mol}^{-1}$), C_{O_2} is the concentration of oxygen dissolved ($1.1 \times 10^{-6} \text{ mol cm}^{-3}$), D_{O_2} is the diffusion coefficient of O₂ in the bulk solution ($1.9 \times 10^{-5} \text{ cm}^2 \text{ s}$), and v is the kinetic viscosity of the solution ($1.0 \times 10^{-2} \text{ cm}^2 \text{ s}$). The Koutecky-Levich plots for the ORR on both Fe-N/C-TsOH-600 and Fe-N/C-600 at three different electrode potentials (-0.20 , -0.40 , and -0.60 V) are shown in Fig. 2(c) and (d). Based on these plots, we can see that:

The average n values were determined to be 3.098 for Fe-N/C-600 and 3.899 for Fe-N/C-TsOH-600, the latter being very close to 4. Clearly, the catalysts doped with TsOH show a much higher overall ORR electron number than those without TsOH doping, indicating a significant difference in the mechanisms they catalyze. In other words, the ORR catalyzed by Fe-N/C-TsOH-600 is a 4-electron transfer process from O₂ to H₂O, whereas Fe-N/C-600 generally tends to catalyze the ORR through a (2+2)-electron pathway, producing H₂O₂, which is capable of oxidizing and splitting active sites.

The intercepts for all the Koutecky-Levich plots are slightly higher than 0. A non-zero intercept for a Koutecky-Levich plot demonstrates that the reaction can occur within the pores of the catalyst rather than just on the top surface exposed to the bulk solution, thus increasing the active surface area at slower kinetics and thereby affecting the slope.^{25,26} Therefore, it can be concluded that the ORR catalyzed by Fe-N/C-TsOH-600 is much faster than that catalyzed by Fe-N/C-600.

As the potential increases, the Koutecky-Levich slope increases for both catalysts, suggesting a decrease in the number of electrons transferred during the ORR and, thus, a reduction in H₂O selectivity. In addition, the intercepts of the Koutecky-Levich plots become much greater than 0, suggesting a decrease in the kinetics of the catalyst for the ORR. However, the Koutecky-Levich slopes at different electrode potentials for Fe-N/C-TsOH-600 all are much quicker than those for Fe-N/C-600. This further demonstrates that the Fe-N/C has a large active surface area and uniform dispersion of the catalyst on the electrode surface after TsOH doping, hence the faster kinetics for the ORR catalyzed by Fe-N/C-TsOH-600 compared to Fe-N/C-600.

Furthermore, we measured the polarization curves using the RDE technique in O₂-saturated 0.1 mol L⁻¹ KOH solution for catalysts pyrolyzed from 200 to 700°C, with the unpyrolyzed catalyst sample (Fe-N/C-TsOH) for comparison, to clarify the effect of thermal treatment on the ORR activity. The results are presented in Fig. 3. Evidently, the pyrolyzed catalyst samples all show better ORR activities than the unpyrolyzed sample, which is consistent with the common belief that thermal treatment can effectively improve catalysts' ORR activity.^{22,27,28} With increasing pyrolysis temperature, the

ORR activity keeps rising up to 600°C, then starts to decrease at higher temperatures. This suggests that 600°C may be the optimal heat-treatment temperature for obtaining the most electroactive catalyst. Below 600°C, more Fe-N_x active sites can be produced by increasing the pyrolysis temperature. However, above 600°C, for example, at 700°C, the structure of the catalyst will collapse. At the same time, undesirable secondary species will form, possibly leading to a reduced concentration of Fe-N_x moieties on the catalyst surfaces, as indicated by the XRD results below.

3.2. Electrode catalyst loading optimization with respect to the ORR activity

It is expected that increasing the non-noble metal catalyst loading inside the catalyst layer should be an effective way to improve ORR activity and performance.²⁹ Therefore, we used the RDE technique to further investigate the loading effect on ORR activity in an O₂-saturated 0.1 mol L⁻¹ KOH solution. According to our current work, the Fe-N/C-TsOH catalyst obtained by pyrolysis at 600°C would yield the highest ORR catalytic activity. So, to study the catalyst loading effect on ORR activity, Fe-N/C-TsOH-600 catalyst was used to prepare catalyst layers with different loadings (50.9, 101, 203.6, 305.4, and 407.2 mg cm⁻²). The resulting current-potential curves are shown in Fig. 4(a). Increasing the catalyst loading at the disk from 50.9 mg cm⁻² to 407.2 mg cm⁻² yields a much-improved half-potential ($E_{1/2}$) and current density (i_d). In the catalyst loading range of 50 to 400 mg cm⁻², the monotonic increase in ORR activity with increasing catalyst loading suggests that the electrochemically active Fe site density (or concentration) plays an effective role in the catalyst layer in terms of ORR activity enhancement.³⁰ It is understandable that when the electrochemically active Fe site density rises, there are more neighboring catalyst active centers available for H₂O₂ to be further reduced to H₂O, leading to a larger proportion of 4-electron pathway reactions in the whole ORR process through a (2+2)-electron series pathway.²⁹ On the other hand, the ORR rate will be boosted as the loading increases, because the sites participate in the ORR process through an inner sphere mechanism to form O₂-metal adducts such as O₂-Fe-N_x. Another factor may be related to the catalyst layer thickness. The catalyst layer is thicker at a high catalyst loading than at a low one; thus, the H₂O₂ generated in the former case may have more time to stay within the catalyst layer to find another active site for further reduction before its release to the electrolyte, as shown in Fig. 4(b).

3.3. Effect of KOH concentration

Electrocatalysis in alkaline media is a subject of growing industrial importance for fuel cells, since the ORR occurs more readily in alkaline electrolytes than in acidic or neutral electrolytes. For the purpose of practical applications, we studied our catalyst's activity toward the ORR in electrolytes containing various concentrations of KOH, to see how the catalyst activity changed with increasing KOH concentration. Fig. 5(a) presents the polarization curves for the ORR on an electrode in O₂-saturated KOH electrolyte of various concentrations, from 0.1 to 5 mol L⁻¹. We can see that:

(1) The catalyst has a relatively well-defined diffusion-limiting current plateau in all tested KOH electrolytes in the potential range of $-0.76 \sim -0.3 \text{ V}$, which means that the current density is limited by O₂ diffusion from the solution to the electrode surface. Furthermore, the distribution of active sites on the electrode surface is uniform.

(2) Increased KOH concentration resulted in a large shift of the onset potential to a more negative value, with a large decrease in current densities in the kinetic, mixed, and diffusion-limiting regions. Clearly, the diffusivity and solubility of oxygen in KOH electrolytes can significantly contribute to the mass transfer effect of oxygen diffusion through the solution, thus affecting the current densities.

Fig. 5(b) shows the Koutecky-Levich plots obtained at -0.60 V for three different KOH concentrations (0.1 , 1.0 , and 3.0 mol L $^{-1}$). From the slopes of the three lines, the overall electron numbers can be obtained, which are, respectively, 3.9910 , 3.9738 , and 3.9612 . These values are fairly close to 4.0 , indicating that the ORR catalyzed by Fe-N/C-TsOH catalyst is a 4-electron transfer process from O $_2$ to H $_2$ O in all three KOH solution concentrations.

3.4. Electrocatalytic stability

The electrocatalytic stability of catalysts is an important parameter for their practical application. Fig. 6(a) shows the linear potential scan curves of Fe-N/C-TsOH-600 in O $_2$ -saturated 0.1 mol L $^{-1}$ KOH at an electrode rotation speed of 1500 r min $^{-1}$ after CV with different numbers of scans, as indicated. A potential cycling test was carried out between -0.8 and 0.3 V in N $_2$ -saturated 0.1 mol L $^{-1}$ KOH with a potential scan rate of 50 mV s $^{-1}$. The polarization curves were measured before and after 1500 , 4800 , and 6000 cycles in O $_2$ -saturated 0.1 mol L $^{-1}$ KOH using a potential scan rate of 5 mV s $^{-1}$ and an electrode rotation rate of 1500 r min $^{-1}$. A negative shift in both half-wave potential and current density during the first 1500 cycles of potential cycling is shown in Fig. 6(a). But the catalyst performance stabilizes during the last 4800 cycles, without further ORR activity change, indicating that the surface properties of the catalyst are maintained during cycling. Generally, there are two distinct performance degradation stages for a non-precious metal catalyst: an initial higher decay rate and a subsequent lower one. Therefore, the potential cycling method may be a promising protocol to quickly evaluate the stability of a non-precious metal catalyst. To clearly assess the catalyst's stability properties, we calculated the percentage of current density loss, $i_{\text{loss}}\%$, at different potentials, as summarized in Fig. 6(b). The $i_{\text{loss}}\%$ is expressed as follows:

$$i_{\text{loss}}\% = (i_{\text{ini}} - i) / i_{\text{ini}} \times 100\% \quad (2)$$

The $i_{\text{loss}}\%$ of the ORR on the catalyst rises exponentially as the amount of potential cycling increases. This may indicate some intrinsic relationship between the active sites in the catalyst and the kinetics of the ORR. However, further experimental and modeling research is needed to clarify this relationship.

Furthermore, the Fe-N/C-TsOH-600 catalyst was leached in 0.5 mol L $^{-1}$ H $_2$ SO $_4$ to remove excess metals on the catalyst surface, then put it through a second heat treatment at 600°C under N $_2$ for 2 hours. Fig. 7(b) shows the polarization curves for oxygen reduction on Fe-N/C-TsOH catalysts subjected to different conditions. The measurements were conducted in O $_2$ -saturated 0.1 mol L $^{-1}$ KOH using a potential scan rate of 5 mV s $^{-1}$ and an electrode rotation rate of 1500 rpm. It is evident that all samples are catalytically active toward oxygen reduction. The re-pyrolyzed catalyst shows better catalytic activity than the others. Additionally, the onset potential of the ORR on Fe-N/C-TsOH-600 is as high as 50 mV. Leaching in 0.5 mol L $^{-1}$ H $_2$ SO $_4$ for a short while causes a positive shift in the onset potential of Fe-N/C-TsOH-600L and Fe-N/C-TsOH-600LH to

54 mV and 121 mV, respectively. It maybe that species less active toward the ORR, such as Fe $_3$ O $_4$, dissolved in the 0.5 mol L $^{-1}$ H $_2$ SO $_4$ and at the same time increased the surface area of the catalyst. As well, re-pyrolysis is apt to form sites that are much more active and to allow uniform dispersion and stable distribution of the metal on Vulcan XC 72R, thereby improving the electrocatalytic activity of Fe-N/C-TsOH-600LH.

The complete set of oxygen reduction currents on Fe-N/C-TsOH in 0.1 mol L $^{-1}$ KOH, detected at the disk electrode, is summarized in Fig. 7(a). Hydrogen peroxide produced in the course of the ORR was detected by utilizing the ring electrode in the collection mode. The potential of the ring electrode was set at 1.2 V, i.e., the potential at which H $_2$ O $_2$ oxidation proceeds as a diffusion-limited process. Peroxide production (in %) is calculated from the ring-disk measurements, according to the following equation:³¹

$$\chi_{\text{H}_2\text{O}_2}(\%) = 100 [(2i_{\text{ring}} / N) / (i_{\text{disk}} + i_{\text{ring}} / N)] \quad (3)$$

where the collection efficiency is $N = 0.22 \pm 5\%$. The amount of peroxide produced is displayed in Fig. 7(a). In the potential region between -0.8 and 0.2 V, the amount of peroxide is very small (less than 5%), indicating that the ORR proceeds almost entirely through the 4-electron pathway. This 4-electron reduction is confirmed by analysis of the Levich plots, i.e., from the linear dependence of the slopes of i^{-1} versus $\omega^{-1/2}$, shown in Fig. 7(c).

3.5. Electrocatalytic selectivity in the presence of methanol

In a direct methanol fuel cell system, particularly with Pt-based fuel cell catalysts, methanol crossover to the cathode is one of the most significant problems because of the resulting mixed potential, which directly causes losses in efficiency and power density. Thus, it is desirable to develop electrocatalysts with a high selectivity towards oxygen reduction in a system containing methanol. We therefore also investigated ORR activity in the presence of methanol on Fe-N/C-TsOH-600 and Pt/C, and the effect of different methanol concentrations on the ORR performance of both catalysts. Fig. 8 presents the ORR curves of these two catalysts in O $_2$ -saturated 0.1 mol L $^{-1}$ KOH containing 0 , 0.5 , 1.0 , and 5.0 mol L $^{-1}$ methanol, at an electrode rotation speed of 1500 rpm and room temperature. Clearly, the Pt/C catalyst favors the methanol oxidation reaction over the ORR, compared with Fe-N/C-TsOH-600. In methanol-free electrolyte, no methanol-oxidation current is found for either of the catalysts. However, when the methanol concentration is changed from 0 to 5 mol L $^{-1}$, the onset potential shifts from 250 to -220 mV (Fig. 8(a)). The competitive adsorption of oxygen and methanol molecules on the surface of Pt/C results in a mixed potential. The electrode reaction was dominated by oxidation at high molecular concentrations, which limited the dissolved oxygen because Pt/C is active for both oxygen and methanol. In the case of Fe-N/C-TsOH-600, the ORR onset potential and current density change very little with or without the presence of methanol, up to 5.0 mol L $^{-1}$ (Fig. 8(b)). At -2 mA cm $^{-2}$, however, the potential shifts from -131 to -220 mV, indicating that species in a methanol solution within an alkaline medium disrupt the ORR. Nevertheless, our results show that in 0.1 mol L $^{-1}$ KOH, this new material has a relatively higher selectivity towards the ORR in the presence of methanol than does Pt/C, although Fe-N/C-TsOH-600 does not have complete methanol tolerance.

3.5. Morphology and structure of the prepared catalysts

Fig. 9 shows X-ray diffraction spectra of non-pyrolyzed

and pyrolyzed Fe-N/C-TsOH catalysts (at 600 and 700°C, respectively). The spectra exhibit the diffraction characteristics of the carbon support, with a broad shoulder in the range of 20° to 30° for 2θ. From Fig. 9 it can be seen that Fe-N/C-TsOH-RT shows quite strong diffraction peaks due to the crystalline nature of FeSO₄·7H₂O. These peaks disappear after high-temperature treatment. In their place, additional diffraction signals form at 600 and 700°C, which may be due to the generation of metallic iron (α-Fe), iron carbide (Fe₃C), and iron oxide-like magnetite (Fe₃O₄), as well as FeS, respectively.³² These results indicate that the structure of the Fe (II)-PPy precursor complex may have decomposed during the pyrolysis process, and those species could be types of ORR active sites, although with much less activity than is expected for Fe-N_x sites.³⁵ It is notable that Fe-N/C-TsOH pyrolyzed at 700°C exhibits very similar peaks to the catalyst pyrolyzed at 600°C, except that: (1). the shape of these peaks of α-Fe, Fe₃C, and Fe₃O₄ for Fe-N/C-TsOH-700 become much stronger and sharper than for Fe-N/C-TsOH-600. Evidently, due to the formation of these less active species, the quantity of ORR active sites is reduced, thus resulting in less ORR activity for the Fe-N/C-TsOH-700;³⁰ (2). When the samples further heat-treated at 700°C, the diffraction signals of FeS were weakened, indicated that these FeS species maybe contribute to promote the ORR, somehow. So, to avoid the formation of additional species with less ORR activity, the thermal temperature should be below 700°C for a Fe-N/C-TsOH precursor.

To obtain information about the surface atomic composition of the pyrolyzed samples, XPS analysis was performed for unpyrolyzed samples and samples pyrolyzed at 600 and 700°C. The broad scan of all three catalysts showed the peaks associated with C, N, O, S, and Fe. This result agrees with the EDX analysis.

The N 1s and S 2p core levels of the catalysts were recorded for both unpyrolyzed and pyrolyzed Fe-N/C-TsOH samples. Fig. 10(a, b, and c) show the N 1s binding energy region, where the peaks of N 1s at 398.9, 400.5, and 401.3 eV can be attributed to pyridinic N, pyrrolic N, and graphitic N, respectively.³⁴⁻³⁶ From Fig. 10(a), the deconvolution of N signals for unpyrolyzed Fe-N/C-TsOH can be divided into two peaks, corresponding to pyridinic and pyrrolic N. When the thermal treatment temperature is increased to 600°C, more of the pyridinic N transforms into pyrrolic N, such that at 600°C, the fraction of pyrrolic N groups is the larger of the two; this catalyst exhibits higher activity than the unpyrolyzed catalyst, as was shown by the CV and RDE results in Fig. 1. This indicates that the pyrrolic N group is more active for oxygen reduction, and the catalyst pyrolyzed at 600°C has more active sites (pyrrolic N) to facilitate oxygen adsorption. In addition, the preferred protonation of pyridinic sites may explain why pyrolysis at high temperatures leads to more pyrrolic N and less pyridinic N, resulting in more stable catalysts.³⁷ Furthermore, when the Fe-N/C-TsOH samples were heat treated at 700°C, deconvolution of the N signals gave three bands that could be assigned to pyridinic, pyrrolic, and graphitic N, respectively. The pyrrolic N peak is weaker than the one presented in Fig. 10(b), which agrees very well with earlier reports identifying pyrrolic N as responsible for the unique activity of Fe-containing catalysts.³⁸

Fig. 10(d) presents the S 2p spectra measured for the unpyrolyzed catalyst sample (Fe-N/C-TsOH). It can be seen that the catalyst without thermal treatment shows a large band at 167.0–171.0 eV, which can be assigned to the sulfate in the

catalyst precursor.^{22,39} After pyrolysis at 600°C (Fe-N/C-TsOH-600), the deconvolution of the S signals gave two bands with binding energies of 163.8 eV and 168.8 eV, respectively, as shown in Fig. 10(e). These peaks can be attributed to the binding sulfurs in C-S_(n)-C (n = 1 or 2) bonds (60%) and oxidized -SO_(n)- bonds (40%), which are expected to occur at the edges of carbon.⁴⁰ Guo *et al.* found that the -C-S-C- structure is an important factor for optimizing ORR performance.²⁰ This fact may explain why our catalyst pyrolyzed at 600°C shows better catalytic ORR activity. It is believed that pyrolysis of the catalyst in the presence of sulfur could lead to mainly amorphous carbon, resulting in increased catalyst porosity and, in turn, enhanced catalyst performance.^{22,24} As well, the sulfur group doped into M-N_x-C might be helpful for entrapping M ions in an environment rich in pyrrole-type nitrogen. Therefore, it can be concluded that both sulfur doping and nitrogen doping of carbon play key roles in improving electrocatalytic activity for the ORR. For the samples pyrolyzed at higher temperatures, the S 2p peak can be fitted with four different sulfur moieties.⁴¹ The major contributions at binding energies around 163.8 eV (35%, lower 60%), 165.0 eV (30%), and 168.8 eV (30%) can be attributed to the binding sulfurs in C-S_(n)-C (n = 1 or 2) bonds, conjugated -C=S- bonds, and -SON-. The remaining contribution at around 162.1 eV (5%) can be assigned to the reduced (-SH) sulfur moieties. The appearance of -C=S- and -SH reduced the amount of C-S-C, which is why Fe-N/C-TsOH-700 shows lower activity than the catalyst pyrolyzed at 600°C. As mentioned above, both N and S play an important role in improving ORR activity, with pyrrolic N and C-S-C possibly serving as the ORR catalytic sites.

4. Conclusions

Nitrogen/sulfur co-doped carbon materials were explored as non-precious metal catalysts for the ORR in alkaline media. They showed promising catalytic activity towards the ORR along a 4-electron transfer pathway in the overall reaction, and higher tolerance to methanol in comparison to commercial Pt/C catalyst in 0.1 mol L⁻¹ KOH.

The N and S dual-doped catalyst exhibited higher catalytic activity for oxygen reduction in alkaline media than one doped only with N, in terms of onset potential, half-wave potential, and diffusion-limited current density values. In addition, the catalytic activities were strongly dependent on the pyrolysis temperature used in catalyst synthesis, with the best ORR performance obtained at 600°C. Instrumental analysis and XRD and XPS results all showed that 600°C may be the optimal temperature for gaining more Fe-N_x active sites, where the pyrrolic N groups are the most active. Sulfur species structurally bound to carbon in the forms of C-S-C and oxidized -SON- bonds play the key roles in improving ORR activity.

Acknowledgements

This work was supported by the National Natural Science Foundation of China (No. 91223202), the International Science & Technology Cooperation Program of China (No. 2011DFA73410), the Tsinghua University Initiative Scientific Research Program (No. 20101081907), and the National Key Basic Research Program of the China-973 Program (No. 2011CB013102).

Notes and references

- ^a State Key Laboratory of Tribology, Tsinghua University, Beijing 100084, China.
- ^b Shenzhen Key Laboratory of Micro/nano Manufacturing, Research Institute of Tsinghua University in Shenzhen, Shenzhen 518057, China
Email: xl0522@126.com, pangs@tsinghua.edu.cn.
Fax: +86 0755 2695 7008, Tel: +86-755-2671 1824.
- 1 R. Dillon, S. Srinivasan, A.S. Arico, V. Antonucci. *J. Power Sources*, **2004**, 127, 112;
 - 2 J.-L. Qiao, L. Xu, L. Ding, P.-H. Shi, L. Zhang, R. Baker, J.-J. Zhang. *Int. J. Electrochem. Sci.*, **2013**, 8, 1189;
 - 3 S. Liu, H. Zhang, Z. Xu, H. Zhong, H. Jin. *Int. J. Hydrogen Energ.*, **2012**, 37, 19065;
 - 4 K. Gong, F. Du, Z. Xia, M. Durstock, L. Dai. *Science*, **2009**, 323: 760;
 - 5 S. Wang, D. Yu, L. Dai. *J. Am. Chem. Soc.*, 2011, 133, 5182;
 - 6 F. Charreteur, F. Jaouen, J. P. Dodelet. *Electrochim. Acta*, **2009**, 54, 6622;
 - 7 C.-W.-B. Bezerra, L. Zhang, H. Liu, K. Lee, A.-L.-B. Marques, E.-P. Marques, H. Wang, J. Zhang. *J. Power Sources*, **2007**, 173, 891;
 - 8 C.-H. Wang, H.-C. Hsu, S.-T. Chang, H.-Y. Du, C.-P. Chen, J.-C.-S. Wu, H.-C. Shih, L.-C. Chen, K.-H. Chen. *J. Mater. Chem.*, **2010**, 20, 7551;
 - 9 J.-S. Yu, M.-S. Kim, J.-H. Kim. *Phys. Chem. Chem. Phys.*, **2010**, 12, 15274;
 - 10 D. Xia, S. Liu, Z. Wang, G. Chen, L. Zhang, L. Zhang, S. Hui, J. Zhang. *J. Power Sources*, **2008**, 177, 296;
 - 11 C.-H. Wang, S.-T. Chang, H.-C. Hsu, H.-Y. Du, J.-C.-S. Wu, L.-C. Chen, K.-H. Chen. *Diamond Relat. Mater.*, **2011**, 20, 322;
 - 12 B. Merzougua, A. Hachimia, A. Akinpelu, S. Bukola, M. Shao. *Electrochim. Acta*, **2013**, 107, 126;
 - 13 F. Jaouen, V. Goellne, M. Lefèvre, J. Herranz, E. Proietti, J.-P. Dodelet. *Electrochim. Acta*, **2013**, 87, 619;
 - 14 R. Jiang, D. Chu. *J. Electrochem. Soc.*, **2000**, 147, 4605;
 - 15 D. Chu, R. Jiang. *Solid State Ionics*, **2002**, 148, 591;
 - 16 R. Holze, I. Vogel, W. Vielstich. *J. Electroanal. Chem.*, **1986**, 210, 277;
 - 17 L. Yang, S. Jiang, Y. Zhao, L. Zhu, S. Chen, X. Wang, Q. Wu, J. Ma, Y. Ma, Z. Hu. *Angew. Chem. Int. Ed.*, **2011**, 50, 7132;
 - 18 Z. Liu, F. Peng, H. Wang, H. Yu, J. Tan, L. Zhu. *Catal. Commun.*, **2011**, 16, 35;
 - 19 D. Deak, E.-J. Biddinger, K.-A. Luthman, U.-S. Ozkan. *Carbon*, **2010**, 48, 3635;
 - 20 H. Wang, X. Bo, Y. Zhang, L. Guo. *Electrochim. Acta*, **2013**, 108, 404;
 - 21 R. Ahmadi, M. K. Amini, J.-C. Bennett. *J. Catal.*, **2012**, 292, 81;
 - 22 J. Qiao, L. Xu, L. Ding, L. Zhang, R. Baker, X. Dai, J. Zhang. *Appl. Catal., B: Environ.*, **2012**, 125, 197;
 - 23 U.I. Kramm, I. Herrmann, S. Fiechter, G. Zehl, I. Zizak, I. Abs-Wurmbach, J. Radnik, I. Dorbandt, P. Bogdanoff. *ECS Transactions*, **2009**, 25, 659;
 - 24 I. Herrmann, U. I. Kramm, J. Radnik, S. Fiechter, P. Bogdanoff. *J. Electrochem. Soc.*, **2009**, 156, 1283;
 - 25 P.-H. Matter, L. Zhang, U.-S. Ozkan. *J. Catal.*, **2006**, 239, 83;
 - 26 H.-J. Zhang, Q.Z. Jiang, L. Sun, X. Yuan, Z.-F. Ma. *Electrochim. Acta*, **2010**, 55, 1107;
 - 27 G. Hinds. *NPL Report DEPC-MPE*, **2005**, 019, 10;
 - 28 C.-W.-B. Bezerra, L. Zhang, K. Lee, H. Liu, J. Zhang, Z. Shi, A.-L.-B. Marques, E.-P. Marques, S. Wu, S. Wu, J. Zhang. *Electrochim. Acta*, **2008**, 53, 7703;
 - 29 F. Charreteur, S. Ruggeri, F. Jaouen, J.-P. Dodelet. *Electrochim. Acta*, **2008**, 53, 6881;
 - 30 L. Wang, L. Zhang, J. Zhang. *Electrochem. Commun.*, **2011**, 13, 447;
 - 31 B.-B. Blizanac, P.-N. Ross, N.-M. Markovic. *Electrochim. Acta*, **2007**, 52, 2264;
 - 32 A. Velazquez-Palenzuela, L. Zhang, L. Wang, P.-L. Cabot, E. Brillas, K. Tsay, J. Zhang. *Electrochimica Acta*, **2011**, 56, 4744;
 - 33 F. Jaouen, J.-P. Dodelet. *Electrochim. Acta*, **2007**, 52, 5975;
 - 34 H. Wang, T. Maiyalagan, X. Wang. *ACS Catal.*, **2012**, 2, 781;
 - 35 G. Liu, X. Li, P. Ganesan, B.-N. Popov. *Electrochim. Acta*, **2010**, 55, 2853;
 - 36 G. Liu, X. Li, P. Ganesan, B.-N. Popov. *Appl. Catal. B: Environ.*, **2009**, 93, 156;
 - 37 G. Wu, K. Artyushkova, M. Ferrandon, J. Kropf, D. Myers, P. Zelenay. *ECS Transactions*, **2009**, 25, 1299;
 - 38 G. Wu, Z. Chen, K. Artyushkova, F.-H. Garzon, P. Zelenay. *ECS Transactions*, **2008**, 16, 159;
 - 39 L. Zhu, D. Susac, M. Teo, K.-C. Wong, P.-C. Wong, R.-R. Parsons, D. Bizzotto, K. A.-R. Mitchell, S.-A. Campbell. *J. Catal.*, **2008**, 258, 235;
 - 40 Y. Su, Y. Zhang, X. Zhuang, S. Li, D. Wu, F. Zhang, X. Feng. *Carbon*, **2013**, 62, 296;
 - 41 J.-P. Paraknowitsch, B. Wienert, Y. Zhang, A. Thomas. *Chem. Eur. J.*, **2012**, 18, 15416.

Figure captions

Fig. 1 Polarization curves of catalysts doped with and without TsOH in O₂-saturated 0.1 mol L⁻¹ KOH solution. Scan rate: 5 mV s⁻¹. Catalyst loading: 101 μg cm⁻². The insert shows the CVs of the two catalysts in O₂-saturated 0.1 mol L⁻¹ KOH solution. Scan rate: 5 mV s⁻¹.

Fig. 2(a) and (b): Polarization curves for the ORR on Fe-N/C-600 and Fe-N/C-TsOH-600 catalysts, measured in O₂-saturated 0.1 mol L⁻¹ KOH electrolytes at various rotation rates. Potential scan rate: 5 mV s⁻¹. Catalyst loading: 101 μg cm⁻². (c) and (d): Koutecky-Levich plots for Fe-N/C-600 and Fe-N/C-TsOH-600 in O₂-saturated 0.1 mol L⁻¹ KOH solution at potentials of -0.6, -0.4, and -0.2 V, respectively.

Fig. 3 Polarization curves for Fe-N/C-TsOH catalysts pyrolyzed at different heat-treatment temperatures. Measured in O₂-saturated 0.1 mol L⁻¹ KOH solution at a scan rate of 5 mV s⁻¹. Catalyst loading: 101 μg cm⁻².

Fig. 4 (a) Current-Voltage curves recorded on a GC electrode coated by Fe-N/C-TsOH-600 catalyst with several loadings in O₂-saturated 0.1 mol L⁻¹ KOH. Potential scan rate: 5 mV s⁻¹. Electrode rotation rate: 1500 r min⁻¹. Catalyst loading: 101 μg cm⁻². (b) ORR current density (*i*_d) at -0.76 and 0.0 V vs. SHE, respectively, as a function of catalyst loading (data taken from (a)).

Fig. 5 (a) Polarization curves of Fe-N/C-TsOH-600 catalyst in O₂-saturated alkaline solutions with four different KOH concentrations, as marked. Electrode potential scan rate: 5 mV s⁻¹. Electrode rotation rate: 1500 r min⁻¹. Catalyst loading: 101 μg cm⁻². (b) Koutecky-Levich plots at different KOH concentrations.

Fig. 6 (a) Polarization curves for oxygen reduction in O₂-saturated 0.1 mol L⁻¹ KOH on Fe-N/C-TsOH-600 before and after a potential cycling stability test. Scan rate: 5 mV s⁻¹. Electrode rotation rate: 1500 r min⁻¹. Potential cycling was performed in N₂-saturated 0.1 mol L⁻¹ KOH with a scan rate of 50 mV s⁻¹ between -0.8 and 0.4 V vs. SHE for 1500, 4800, and 6000 cycles. (b) Percentage of current density loss, *i*_{loss}%, at different potentials for the ORR in O₂-saturated 0.1 mol L⁻¹ KOH on Fe-N/C-TsOH-600, as a function of the number of potential cycles.

Fig. 7 (a) Percentage of peroxide arising from Fe-N/C-TsOH treated under different conditions: Fe-N/C-TsOH-600, Fe-N/C-TsOH-600L, and Fe-N/C-TsOH-600LH as a function of electrode potential, on the basis of the corresponding RRDE data. (b) Current-potential curves at 298 K for the ORR in O₂-saturated 0.1 mol L⁻¹ KOH solution, on the three kinds of catalysts treated under different conditions. (c) Levich plot at the potential of -0.3 V vs. SHE.

Fig. 8 Polarization curves for O₂ reduction on (a) Pt/C electrode and (b) Fe-N/C-TsOH-600 in O₂-saturated 0.1 mol L⁻¹ KOH electrolyte without and with different concentrations (0.5, 1.0, and 5.0 mol L⁻¹) of methanol solution. Potential scan rate: 5 mV s⁻¹. Electrode rotation rate: 1500 r min⁻¹. Catalyst loading: 101 μg cm⁻².

Fig. 9 X-ray diffraction spectra of non-pyrolyzed and pyrolyzed Fe-N/C-TsOH catalysts at 600 and 700°C, respectively. 1. Fe₃O₄ (022); 2. Fe₃O₄ (113); 3. Fe (011), Fe₃C (013); 4. Fe₃O₄ (115); and 5. Fe₃O₄ (044).

Fig. 10 XPS spectra of deconvoluted N 1s (a, c, and e) and S 2p (b, d, and f) for Fe-N/C-TsOH catalyst. (a), (b): unpyrolyzed; (c), (d): pyrolyzed at 600°C; (e), (f): pyrolyzed at 700°C.

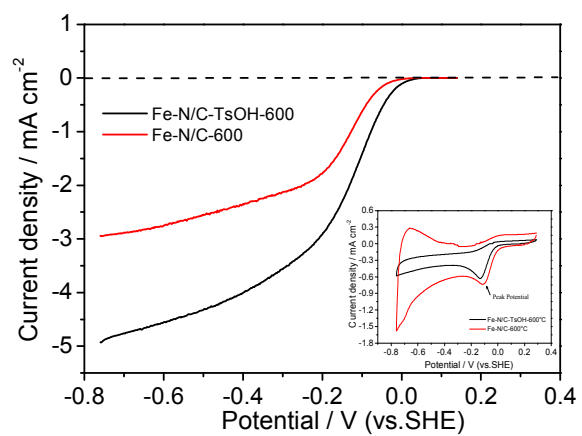


Fig. 1

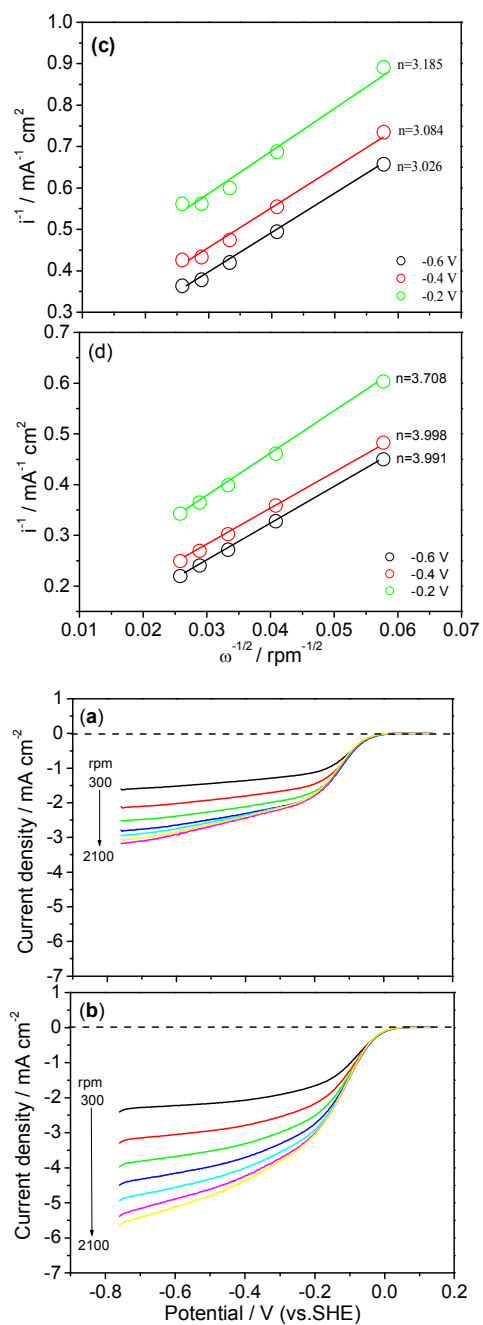


Fig. 2

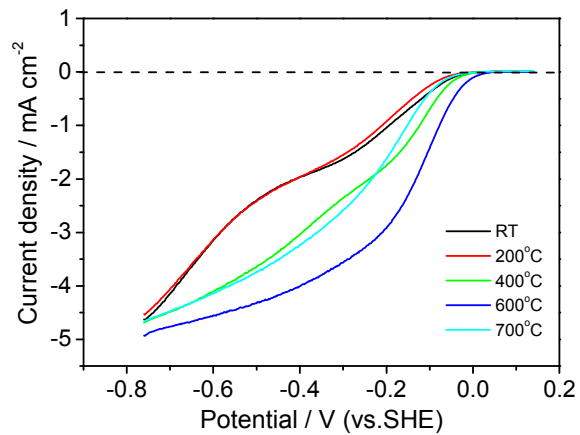


Fig. 3

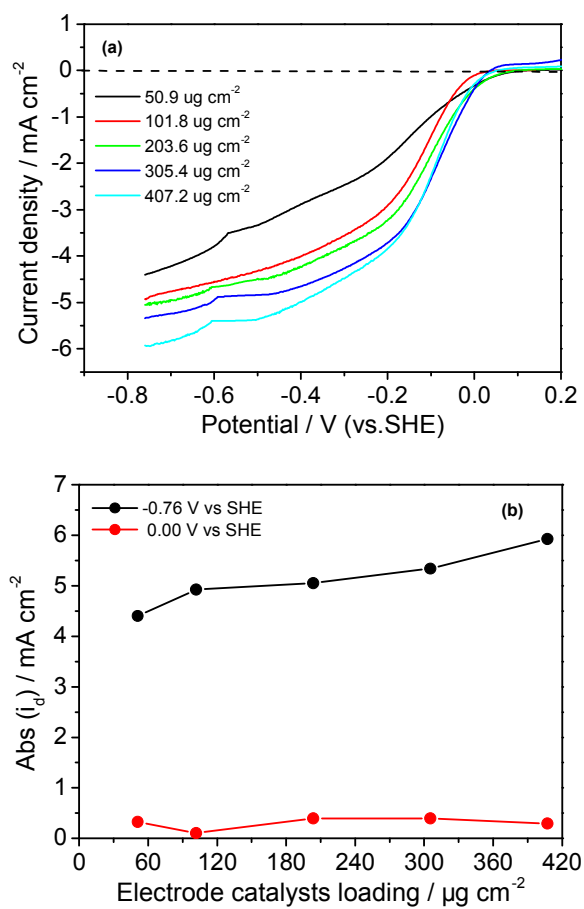


Fig. 4

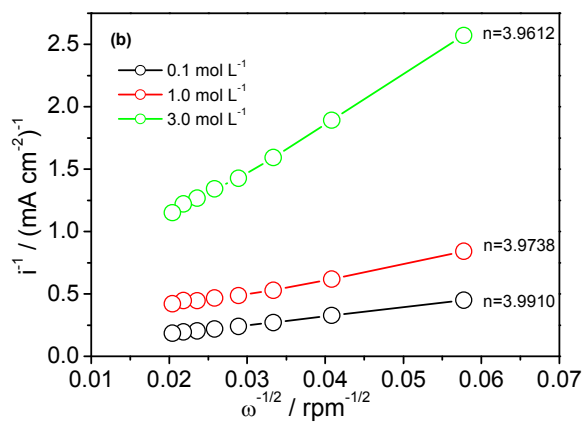
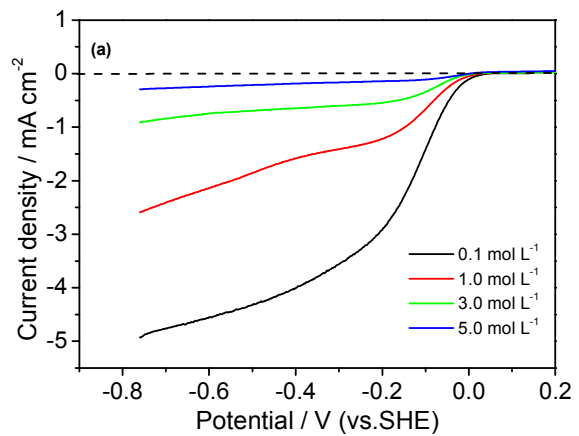


Fig. 5

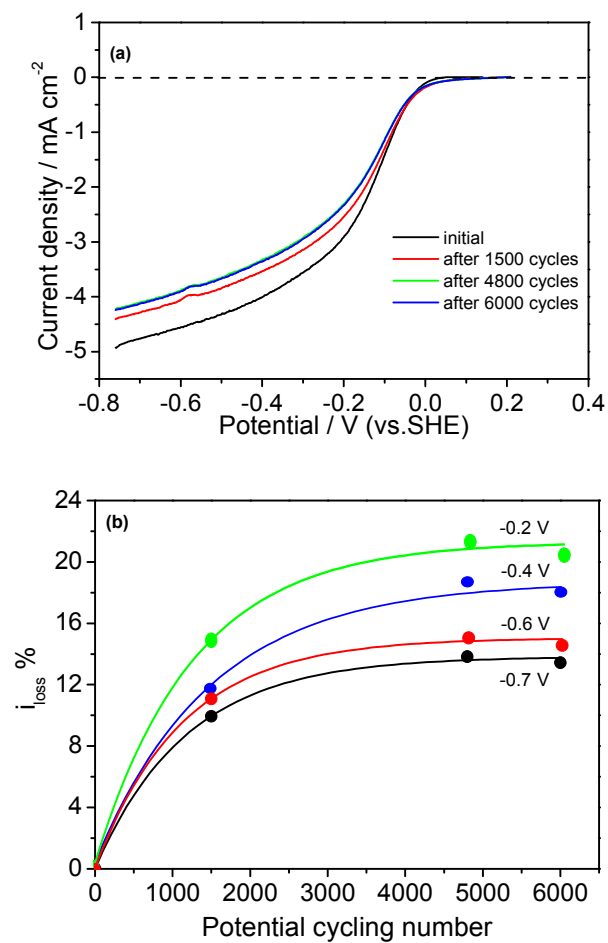


Fig. 6

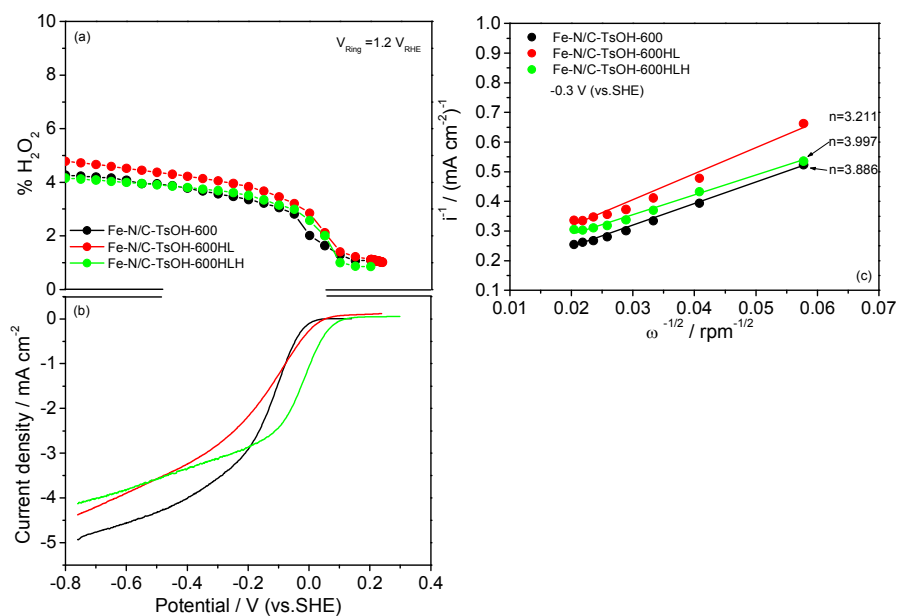


Fig. 7

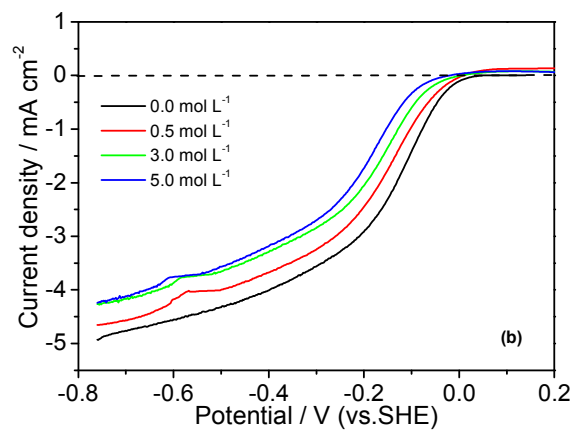
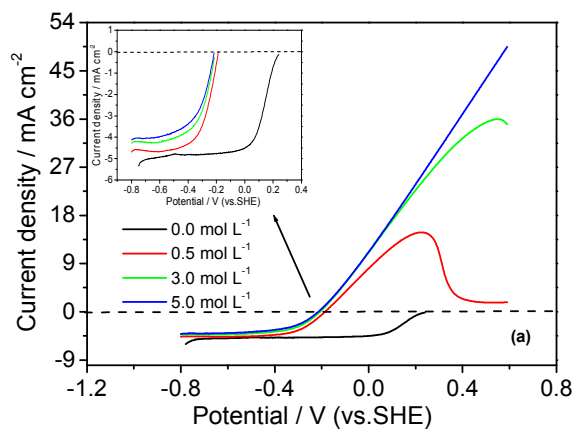


Fig. 8

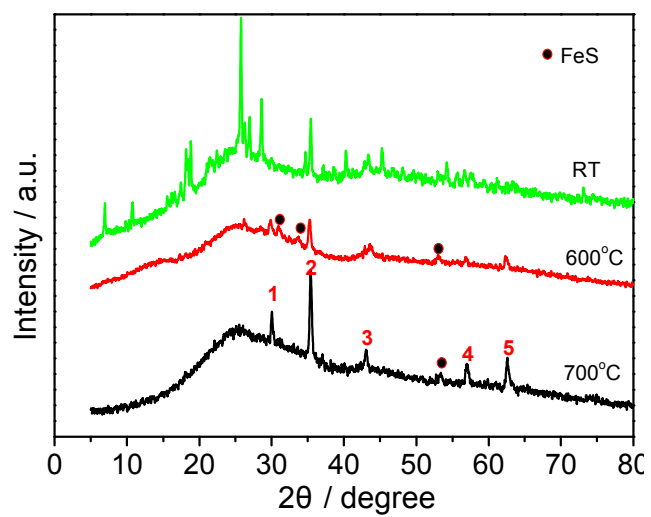


Fig. 9

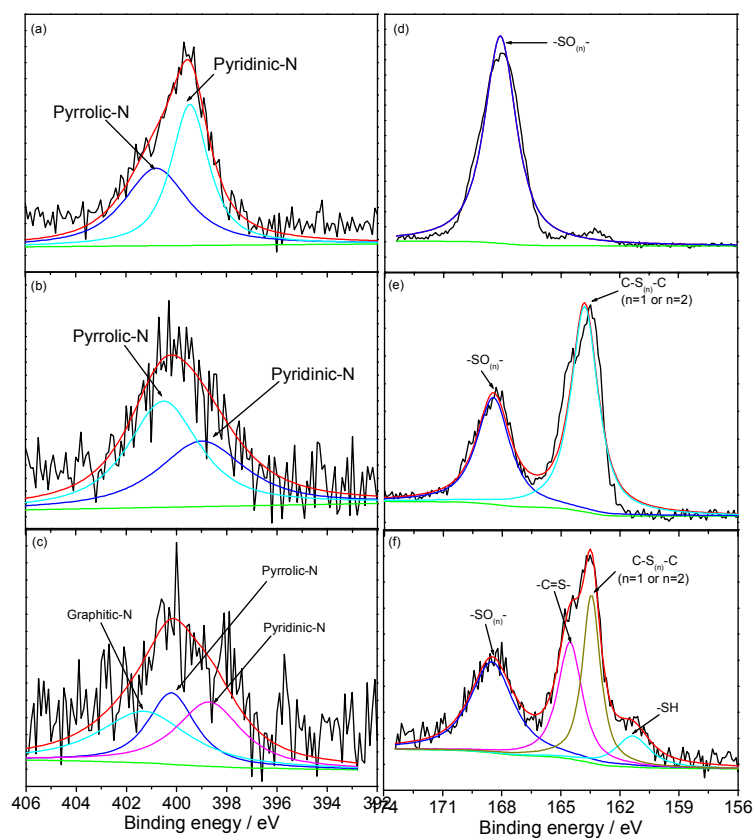


Fig. 10